Proton Momentum Distribution of Liquid Water from Room Temperature to the Supercritical Phase

C. Pantalei,[1] A. Pietropaolo,[1] R. Senesi,[1] S. Imberti,[1] C. Andreani,[1] J. Mayers,[2] C. Burnham,[3] and G. Reiter[3]

[1]*Università degli Studi di Roma "Tor Vergata," Dipartimento di Fisica and Centro NAST (Nanoscienze-Nanotecnologie-Strumentazione), Via della Ricerca Scientifica 1, 00133 Roma, Italy*

[2]*ISIS, Rutherford-Appleton Laboratory, Chilton, Didcot, England*

[3]*Physics Department, University of Houston, Houston, Texas 77204-5506, USA*

(Received 1 August 2007; published 2 May 2008)

Measurements of the proton momentum distribution $n(p)$ in water from ambient conditions to above the supercritical point are compared with theoretical calculations based on a recently developed polarizable water model. The $n(p)$ along the H-bond direction is narrower in the dense phases, and approaches that of the isolated molecule in the more dilute phases. The theoretical model, which includes only electrostatic interactions, is unable to explain the softening of the local potential experienced by the proton in the dense phases, but it accurately predicts the $n(p)$ for the dilute phases.

DOI: 10.1103/PhysRevLett.100.177801 PACS numbers: 61.25.Em, 33.15.Fm, 61.05.F−, 82.30.Rs

Supercritical water is of technological interest for applications as varied as producing hydrogen from glucose [1] and fabricating nanoparticles of yttrium aluminum garnet [2]. Beyond its technological interest, the variation of the properties of water as it is heated under pressure to reach the supercritical point and above provides a means of investigating the effects of the hydrogen bond network on those properties as the network is pulled apart. The spatial distribution of the atoms as this happens has been investigated with neutron and x-ray scattering [3,4], and compared with *ab initio* calculations [5]. The momentum distribution $n(p)$ of the protons in water provides basic information that is complementary to the well studied spatial distributions. It is a local probe that can be used to infer the details of the effective potential the proton sees as the hydrogen bond network changes [6]. To this end, we have measured $n(p)$ at five temperatures and pressures from room temperature water at 1 bar to water at 673 K and 1060 bar, using deep inelastic neutron scattering [7].

The earliest $n(p)$ measurements on supercritical water, by Uffindell *et al.* [8], provided only the average kinetic energy, due to the limitations of the data analysis available at the time. These results were criticized by Andreani *et al.* [9], on the grounds that the subtraction of the sizable background from the pressure cell was not done carefully enough. The data of Uffindell *et al.* were subsequently reanalyzed by Reiter *et al.* [10] to obtain the shape of the $n(p)$, without, however, amending the process of subtraction of the cell signal. On the basis of that data, it was concluded that the Born-Oppenheimer potential in the supercritical phase was actually a double well. Our present results, with longer counting times, and in which the subtraction of the cell signal has been done along the lines suggested in Andreani *et al.*, do not show any evidence of a double well, which we believe to be an artifact of the earlier analysis. Our data can be described as an anisotropic Gaussian, corresponding to effectively harmonic wells. We find that there is significant variation of the $n(p)$ as the experimental conditions are varied. In particular, the $n(p)$ along the stretch direction is significantly narrower in the two dense samples, ambient water and 423 K water with density $\rho = 0.9$ g/cc, than it is in the higher temperature and lower density samples, $T = 523$ K, $\rho = 0.8$ g/cc, $T = 573$ K, $\rho = 0.7$ g/cc, and $T = 673$ K, $\rho = 0.7$ g/cc. In an attempt to understand these differences, we have done path-integral molecular dynamics calculations [11] of the $n(p)$ using a phenomenological potential developed by one of the authors (C. B.) that is an extension of the TTM2-F model to include more accurately the polarizability surface of the water molecule. We think this gives a reasonably accurate account of the electrostatic interactions of the water molecules, but it cannot account for any interactions with the hydrogen bonded oxygen involving electron transfer. The results describe the low density samples to within the experimental error, but cannot reproduce the narrowing of the $n(p)$, associated with the softening of the stretch mode potential, in the higher density samples. We conclude that either we have an inadequate model of the electrostatic interactions or the softening of the potential due to electronic transfer [12,13] is an essential feature of the H-bond network at the higher densities. This softening is a significant contribution to bond energetics, with the reduction in zero point energy from the gas phase accounting for nearly a fifth of the total energy in the bond.

The theoretical basis of deep inelastic neutron scattering (DINS) is the impulse approximation (IA) [6,7]. This approximation treats the scattering event as single atom scattering with conservation of momentum and of kinetic energy of the neutron plus the target atom. The recoil energy, $\hbar\omega_r$, is linked to the hydrogen mass M and to the wave vector transfer q by the relation $\hbar\omega_r = \hbar^2 q^2/2M$. The IA is strictly valid in the limit of $q \rightarrow \infty$, where the neutron scattering function is related to the $n(p)$ by the

relation:

$$S(\vec{q},\omega) = \int n(\vec{p})\delta\left(\omega - \frac{\hbar q^2}{2M} - \frac{\vec{q}\cdot\vec{p}}{M}\right)d\vec{p} = \frac{M}{q}J_{\mathrm{IA}}(\hat{q},y), \quad (1)$$

where $y = \frac{M}{q}(\omega - \frac{\hbar q^2}{2M})$. Moreover, in an isotropic system there is no dependence on $\hat{q}$ and the response function becomes $J_{\mathrm{IA}}(y) = 2\pi\int_{|y|}^{\infty} pn(p)dp$. In order to extract the proton mean kinetic energy, $\langle E_K\rangle$, and the $n(p)$, a general expansion of the response function in Hermite polynomials $H_n(x)$ is used. This expansion can be written in the form:

$$J_{\mathrm{IA}}(y) = \frac{e^{-y^2/2\sigma^2}}{\sqrt{2\pi}\sigma}\left[1 + \sum_{n=2}^{\infty}\frac{a_n}{2^{2n}n!}H_{2n}\left(\frac{y}{\sqrt{2}\sigma}\right)\right]. \quad (2)$$

where σ is the standard deviation and the a_n are the Hermite coefficients. $\langle E_K\rangle$ is related to σ by the formula $\langle E_K\rangle = 3\hbar^2\sigma^2/2M$. $n(p)$ is expressed in terms of the generalized Laguerre polynomials, $L_n^{1/2}$, and of the same Hermite coefficients a_n by [6]

$$n(p) = \frac{e^{-(p^2/2\sigma^2)}}{(\sqrt{2\pi}\sigma)^3}\left[1 + \sum_{n=2}^{\infty}a_n(-1)^n L_n^{1/2}\left(\frac{p^2}{2\sigma^2}\right)\right]. \quad (3)$$

For finite q values, the deviation from IA can be accounted for in terms of additive corrections to the asymptotic form $J(y,q) = J_{\mathrm{IA}}(y) + \Delta J(y,q)$, where $\Delta J(y,q) \approx H_3(y/\sqrt{2}\sigma)/q$.

The DINS measurements have been performed on the VESUVIO instrument at ISIS, with energy transfer between 1 eV and 30 eV and wave vector transfer between 30 Å^{-1} and 200 Å^{-1}. The energy analysis is obtained by a gold foil with a resonance of 4908 meV placed between the sample and the detectors. In this case 31 ^{6}Li glass detectors, positioned between 34.58° and 67.64°, have been used. The cell employed is a high pressure TiZr cell. The contribution of the multiple scattering and of the cell signal have been estimated, respectively, by means of Monte Carlo simulation and by a procedure that accounts for the signal of the empty can. The subtraction of these contributions from the fixed-angle spectra make it possible to extract the hydrogen peak. By the transformation in the y space, it is possible to obtain the experimental fixed-angle response function that is the convolution of $J(y,q)$ with the fixed-angle spectrometer resolution $R(y,q)$. A simultaneous fit of the entire set of fixed-angle spectra has been performed to obtain the best fit parameters of $J_{\mathrm{IA}}(y)$. Table I shows the investigated thermodynamical points, chosen to have a density as constant as possible, together with the results of σ, $\langle E_K\rangle$, and a_2, the latter being the only significant non-Gaussian coefficient. Data have been analyzed also in double difference configuration. The loss in signal intensity allowed us to find only the σ parameter. The $\langle E_K\rangle$ so obtained is in agreement, within the error, with the results reported here.

We find, empirically, that the shape of the Compton profile we measure is unaffected by whatever the mechanism is for the intensity deficit seen for hydrogen relative to heavier nuclei [14,15]. In systems where we know from other measurements what to expect, we observe no distortion [16]. The intensity deficit varies with the transferred momentum. However, the Compton profile from all detectors is the same, for a liquid, despite the large change in the average transferred momentum [17]. We have therefore made no attempt to correct for this effect. In order to interpret the data, simulations were performed using the flexible and polarizable water model of Burnham *et al.* [11]. This model was reparametrized to reproduce the monomer polarizability tensor as a function of geometry, as determined by electronic structure calculations. It is based on the TTM2-F model of Burnham and Xantheas [18], but has a more accurate polarizability surface. Intermolecular interactions are handled using smeared charges and dipoles of Thole, which damp out the electrostatics at short range. In addition, there is an attractive or repulsive Lennard-Jones–like interaction between O sites, fitted to reproduce dimer energetics.

A normal mode path-integral molecular dynamics algorithm was used to calculate equilibrium position [$g(r)$] and momentum distributions. Bulk simulations were performed with 128 water molecules in periodic boundary conditions using an Ewald sum to handle long-range electrostatics. Calculation of the $n(p)$ requires evaluation of off-diagonal density matrix elements for the target particle, tracing over all other particles in the system. In a path-integral simulation, this translates to using an open chain path on the target atom, with all other particles using closed-chain paths. Because the target atom is treated differently from other atoms, it is normally possible to only calculate the $n(p)$ for one atom during the course of a path-integral simulation. However, Morrone *et al.* [19] have recently shown that calculated momentum distribu-

TABLE I. Temperatures, pressures, and densities of experimental points are reported with the experimental and calculated results obtained for σ, $\langle E_K\rangle$, the a_2 coefficient, and the average number of hydrogen bonds, as defined in the text.

Temperature (K)	Pressure (bar)	Density (g/cm^3)	σ (Å^{-1})	E_k (meV)	a_2	σ calc.	a_2 calc.	No. H bonds
300	1	1.0	4.79 ± 0.05	143 ± 3	0.026 ± 0.03	5.15	0.151	3.3
423	100	0.9	4.99 ± 0.05	155 ± 3	0.052 ± 0.04	5.20	0.151	2.6
523	65	0.8	5.21 ± 0.07	169 ± 5	0.101 ± 0.04	5.27	0.139	1.6
573	120	0.7	5.25 ± 0.08	172 ± 5	0.107 ± 0.04	5.27	0.136	1.6
673	1060	0.7	5.36 ± 0.06	178 ± 4	0.083 ± 0.03	5.36	0.114	1.4

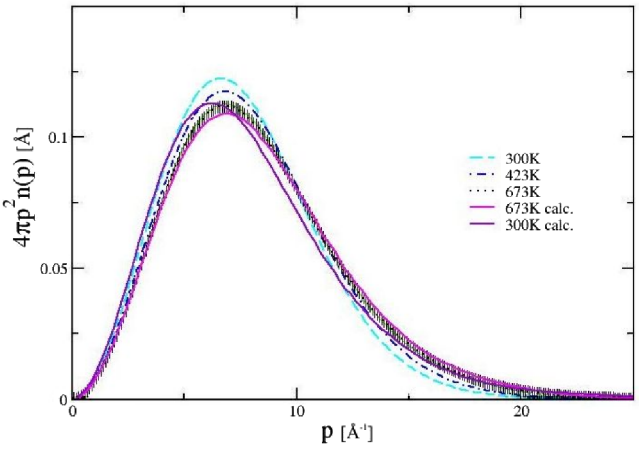

FIG. 1 (color online). Radial proton momentum distribution at several measured temperatures compared with path-integral molecular dynamics calculations using an extended TTM2-F model. Error bars on the lower temperature measurements have been omitted for clarity and are similar to those shown.

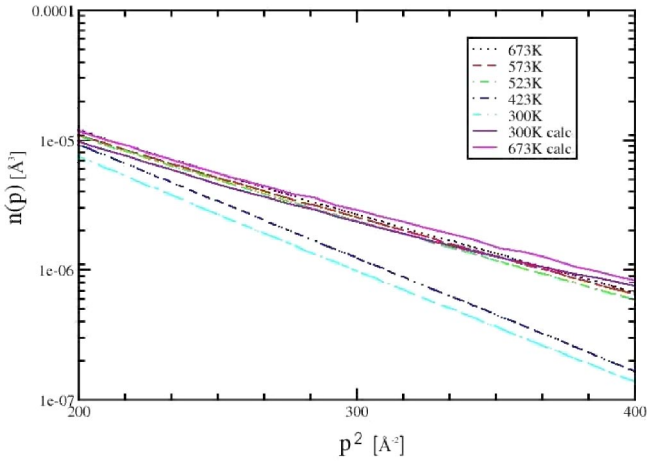

FIG. 2 (color online). The $n(p)$ in the region where it is dominated by the motion in the stretch direction. The calculated distribution at 673 K is in very good agreement with the measured results and is nearly identical to that of the free monomer. The calculated result at 300 K gives too large a momentum width to describe the data. The electrostatic interactions included in the model are unable to account for the softening of the potential of the proton with increasing density.

tions in water are almost unaffected if one open chain per molecule is used, with the advantage that the resulting distribution can be averaged over all open chains in the system. We have adopted their approach in this work. Equilibrium properties were found to be sufficiently converged using an imaginary time slice of interval $\Delta t = \beta\hbar/N \approx 0.8$ fs, where N is the number of replicas. The path-integral calculations were performed using 32 replicas for 300 K water, 24 replicas for 423 K supercritical water, and 16 replicas for 523 K, 573 K, 673 K supercritical water.

In Fig. 1, we show some of the experimental radial momentum distributions, $4\pi p^2 n(p)$, compared with the calculations at 673 K and 300 K. The results at 300 K are consistent with earlier measurements [10]. The errors in all the experiments are similar to those shown for the 673 K data, but have been suppressed for clarity. While the 673 K distribution is reproduced rather well, it can be seen from the figure that the 300 K results are not accurate. In Fig. 2, the momentum distributions are plotted on a logarithmic scale as a function of p^2, in order to exhibit the asymptotic behavior for large p. Since the stretch mode frequency is roughly twice that of the bending modes, and 4 times that of the librational modes [20], the $n(p)$ in a frame attached to an individual water molecule is roughly an anisotropic Gaussian, with the transverse momentum width slightly more than half the width along the stretch mode direction. As a consequence, the spherically averaged momentum distribution, which is what we measure, is determined entirely by motion in the stretch direction at large momentum transfer ($p \geq 10$ Å). The slope of the lines in Fig. 2 is $1/2\sigma_z^2$, where σ_z is the momentum width in the stretch mode direction. We see from Fig. 2 that there is considerable variation in the stretch mode momentum width in going from room temperature to 673 K. We have included in the figure the calculated $n(p)$ for 300 K and 673 K. The value of σ_z as inferred from the low density measurements is essentially the same as that we calculated for a monomer. Our calculations, although accurate for the high temperature measurements, cannot reproduce the lower temperature, higher density results. The electrostatic interactions included in the model, although they do produce a softening of the stretch potential as the density increases (see σ calc and No. H bonds in Table I), are insufficient to produce the softening observed. This is true despite the fact that they give a very good account of the pair correlation functions and vibrational spectrum [11,21]. We show in Fig. 3 the calculated $g_{\mathrm{O\text{-}O}}(r)$ and $g_{\mathrm{O\text{-}H}}(r)$ for 300 K and 673 K compared with the experimental values taken from Soper [22,23]. It is evident that the spatial structure predicted by the model is very close to that observed, over the complete range of temperatures, despite the lack of agreement with the $n(p)$ at the higher densities. This is not surprising, as the slight increase in the spatial width of the proton distribution implied by the narrowing of the momentum distribution has a very minor effect on the spatial distribution of the surrounding particles, but it does point up that there is additional complementary information in the $n(p)$. In as much as the spatial structure in our calculations is reliable, we can calculate the extent to which the H-bond network remains at a given temperature. The definition of a H bond is somewhat arbitrary. Using the definition of a H bond introduced by Wernet *et al.* [24], in which H bonds are determined according to both the intermolecular OO distance and the OHO H-bonding angle, we can calculate the average number of H bonds each molecule participates in, shown in the last column of Table I. For linear bonds, H bonds are counted for O-O separations less than 3.2 Å. The number

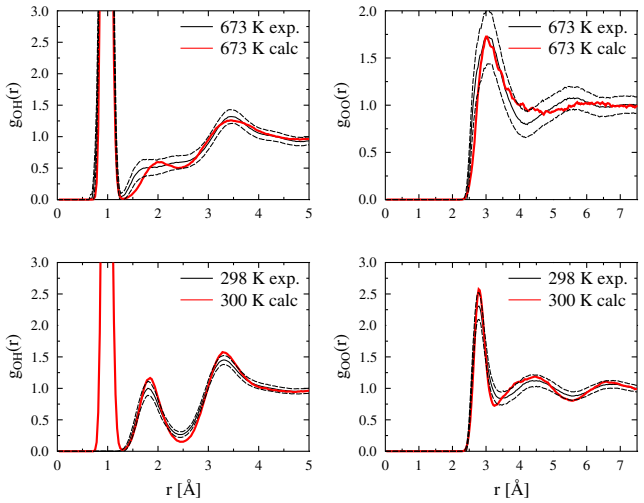

FIG. 3 (color online). Comparison of calculated [gray (red) continuous lines] and measured (black continuous lines, 1 standard deviation errors, dashed lines) radial distribution functions at comparable conditions. The supercritical measured data are case (b) from Ref. [23], while the room temperature data are referred to as "PCCP" joint neutron and x-ray diffraction refinement from Ref. [22]. The theoretical calculation is for a density (0.023 398 molecules/Å^3) that is midway between case (b) (0.0221 molecules/Å^3 and case (c) (0.0245 molecules/Å^3). An overall good agreement is found between measured and calculated distribution functions for ambient and supercritical phases.

of H bonds we find at room temperature is consistent with earlier experimental and theoretical work [25,26]. Evidently, the softening of the ground state potential we have observed for $T = 300$ K and $T = 423$ K is associated with the presence of a more complete H-bond network.

To summarize, we have measured accurately the momentum distribution for protons in water from room temperature to the supercritical phase. We find that our best efforts at producing a model for water that includes accurate electrostatic interactions are insufficient to explain the softening of the proton potential from its values in the supercritical phase to that in ambient water. That the value of the momentum width for the stretch direction is essentially the same in water at 423 K, which still retains a high number of H bonds, as it is in 300 K water, suggests that it is the H bond that is responsible for the softening. While it is possible that more accurate calculations of the electrostatic interactions could reproduce the $n(p)$ in 300 K water, we think this unlikely, and that the experimental results provide clear evidence of an additional softening of the potential of the proton, beyond electrostatic effects, due to electron transfer within the bond. In any case, the reduction in zero point energy of the proton due to the softening of the potential accounts for almost a fifth of the total binding energy of a bond, and hence is a significant factor in the energetics of the H bonds in ambient water.

This work was supported within the CNR-CCLRC Agreement No. 01/9001 concerning collaboration in scientific research at the spallation neutron source ISIS. The work of G. Reiter and C. Burnham was supported by DOE Grant No. DE-FG02-03ER46078. The financial support of the Consiglio Nazionale delle Ricerche and of the Department of Energy in this research is hereby acknowledged.

[1] A. J. Byrd, K. K. Pant, and R. B. Gupta, Ind. Eng. Chem. Res. **46**, 3574 (2007).
[2] A. Cabanas, J. Li, P. Blood, T. Chudoba, W. Lojkowski, M. Poliakoff, and E. Lester, J. Supercrit. Fluids **40**, 284 (2007).
[3] A. Botti, F. Bruni, M. A. Ricci, and A. K. Soper, J. Chem. Phys. **109**, 3180 (1998).
[4] T. Tassaing, M.-C. Bellissent-Funel, B. Guillot, and Y. Guissani, Europhys. Lett. **42**, 265 (1998).
[5] M. Boero, K. Terakura, T. Ikeshoji, C. C. Liew, and M. Parrinello, Phys. Rev. Lett. **85**, 3245 (2000).
[6] G. Reiter and R. Silver, Phys. Rev. Lett. **54**, 1047 (1985).
[7] C. Andreani, D. Colognesi, J. Mayers, G. F. Reiter, and R. Senesi, Adv. Phys. **54**, 377 (2005).
[8] C. H. Uffindell, A. I. Kolesnikov, J.-C. Li, and J. Mayers, Phys. Rev. B **62**, 5492 (2000).
[9] C. Andreani, D. Colognesi, E. Degiorgi, and M. A. Ricci, J. Chem. Phys. **115**, 11243 (2001).
[10] G. F. Reiter, J. C. Li, J. Mayers, T. Abdul-Redah, and P. Platzman, Braz. J. Phys. **34**, 142 (2004).
[11] C. J. Burnham, G. F. Reiter, J. Mayers, T. Abdul-Redah, H. Reichert, and H. Dosch, Phys. Chem. Chem. Phys. **8**, 3966 (2006).
[12] A. Nilsson, H. Ogasawara, M. Cavalleri, D. Nordlund, M. Nyberg, P. Wernet, and L. G. M. Pettersson, J. Chem. Phys. **122**, 154505 (2005).
[13] M. V. Fernandez-Serra and E. Artacho, Phys. Rev. Lett. **96**, 016404 (2006).
[14] C. A. Chatzimidriou-Dreisman, T. Abdul-Redah, R. Streffer, and J. Mayers, Phys. Rev. Lett. **79**, 2839 (1997).
[15] J. Mayers and T. Abdul-Redah, J. Phys. Condens. Matter **16**, 4811 (2004).
[16] A. C. Evans, D. Timms, J. Mayers, and S. M. Bennington, Phys. Rev. B **53**, 3023 (1996).
[17] G. Reiter, C. Burnham, D. Homouz, P. M. Platzman, J. Mayers, T. Abdul-Redah, A. P. Moravsky, J. C. Li, C. K. Loong, and A. Kolesnikov, Phys. Rev. Lett. **97**, 247801 (2006).
[18] C. J. Burnham and S. S. Xantheas, J. Chem. Phys. **116**, 5115 (2002).
[19] J. A. Morrone, V. Srinivasan, D. Sebastiani, and R. Car, J. Chem. Phys. **126**, 234504 (2007).
[20] J. E. Bertie and Z. Lan, Appl. Spectrosc. **50**, 1047 (1996).
[21] F. Paesani, S. Iuchi, and G. A. Voth, J. Chem. Phys. **127**, 074506 (2007).
[22] A. K. Soper, J. Phys. Condens. Matter **19**, 335206 (2007).
[23] A. K. Soper, Chem. Phys. **258**, 121 (2000).
[24] P. Wernet *et al.*, Science **304**, 995 (2004).
[25] S. J. Suresh and V. M. Naik, J. Chem. Phys. **113**, 9727 (2000).
[26] R. Kumar, J. R. Schmidt, and J. L. Skinner, J. Chem. Phys. **126**, 204107 (2007).